

# Gauge Singlet Vector-like Fermion Dark Matter, LHC Di-photon Rate and Unitarity Constraints

Shrihari Gopalakrishna <sup>\*</sup>, Tuhin Subhra Mukherjee <sup>†</sup>,

The Institute of Mathematical Sciences (IMSc), C.I.T Campus, Taramani, Chennai 600113, India.

July 19, 2022

## Abstract

We consider a gauge-singlet vector-like fermion dark matter model that also contains a gauge-singlet scalar and an  $SU(2)$  singlet vector-like quark. The dark matter has a tree-level coupling with the gauge-singlet scalar but communicates with the standard model via loop-level scalar-gluon-gluon and scalar-photon-photon effective couplings induced by the vector-like quark. The main focus of the paper is to study the implications of such effective couplings. We also include the Higgs-portal coupling of the dark matter due to scalar-Higgs mixing. In the model parameter space, we present the dark matter relic-density, the dark-matter-nucleon direct-detection scattering cross-section, the large hadron Collider diphoton resonance signal rate, and the theoretical upper-bounds on the fermion-scalar couplings from perturbative unitarity.

## 1 Introduction

In this work we study the possibility of a standard model gauge-singlet vector-like fermion (VLF,  $\psi$ ) to be a dark matter candidate. The dark matter interacts with the visible standard model (SM) sector through an SM gauge-singlet scalar ( $\phi$ ) which has vector-like quark (VLQ) loop-induced couplings to di-photons and di-gluons, and also possibly via the Higgs portal. The emphasis in this work will be the former loop-induced couplings, with the latter Higgs portal contribution subdominant, which helps evade the somewhat tight LHC di-Higgs channel constraints which forces a small Higgs-singlet mixing. These ingredients could be present in various BSM frameworks and our analysis here could be useful in such settings.

We compute the dark matter relic-density, the dark-matter-nucleon direct-detection cross section, the present direct LHC constraints, the LHC gluon-gluon-fusion rate and the LHC diphoton rate for various total widths of the  $\phi$ , as a function of the effective gluon-gluon-scalar ( $\phi gg$ ) and gamma-gamma-scalar ( $\phi \gamma \gamma$ ) effective couplings. We also present the perturbative unitarity bounds on the  $\phi$  couplings to vector-like fermions. If  $M_\psi < M_\phi/2$ , the  $\phi \rightarrow \psi\psi$  decays contribute to  $\Gamma_\phi$ . We perform our analysis first in a model independent manner that could be useful for many models, and apply it to our model subsequently.

If the  $\phi$  and the SM Higgs ( $h$ ) are coupled via a cubic or quartic interaction, and if there is a non-zero vacuum expectation value of the singlet scalar, the  $\phi$  could mix with  $h$  after electroweak symmetry breaking. This mixing induces a coupling between the dark-matter and  $\phi$  sector and the

---

<sup>\*</sup>shri@imsc.res.in

<sup>†</sup>tuhin@imsc.res.in

standard model (SM) sector. Interestingly, in the model we consider, the visible and hidden sectors do not decouple in the limit of the Higgs-portal mixing going to zero since the effective  $\phi gg$  and  $\phi\gamma\gamma$  couplings induced by VLQ remain as couplings between the two sectors. We investigate these aspects in this work, and find that the Higgs-portal mixing (i.e.  $h \leftrightarrow \phi$  mixing) is constrained to be very small by the present di-Higgs LHC search limits, and therefore our focus in this work is on the VLQ loop-induced scalar mediation possibility. When the Higgs-portal mixing is negligibly small, the  $\psi\psi \rightarrow SM$  self-annihilation process which sets the relic-density in the early universe is mediated by  $\phi$  in the  $s$ -channel, and the interaction of the dark matter with a nucleon that leads to direct-detection signals is mediated by the  $\phi$  in the  $t$ -channel.

We summarize here other studies in the literature that have overlap with our work. A model-independent analysis in the present context is also carried out in Refs. [1, 2, 3]. An analysis of a gauge-singlet fermionic dark matter in the Higgs portal scenario but with significant  $\phi \leftrightarrow h$  mixing is carried out for example in Refs. [4, 5, 6, 7, 8, 9]. The phenomenology of a singlet scalar coupled to VLFs in the context of the earlier 750 GeV di-photon excess [10, 11] which also discuss the dark matter implications of the neutral VLFs present in those models is studied in Refs. [12, 13, 14, 15, 16, 17, 18]. In this work, we study the prospects of a singlet VLF to be dark matter for various dark matter and singlet scalar mediator masses. We also present the constraint on the  $h - \phi$  mixing angle ( $\theta_h$ ) from the LHC  $hh$  channel results [19], which is not analyzed in the references mentioned above. Usually in the literature only the  $h$  mediated processes are included in the dark matter direct-detection cross section calculations. However, for small  $\theta_h$  (or when there is no mixing), the  $h$  mediated processes are suppressed, and the  $\phi$  mediated process due to the  $\phi gg$  and  $\phi\gamma\gamma$  effective coupling induced by VLQs that we analyze here are important. Our results here are relevant in this context. Ref. [16] does include this contribution, although in the context of scalar dark matter, but in their case the dominant contribution is the Higgs-scalar mixing contribution. We also find constraints on the parameter space from the requirement of perturbative unitarity in the  $\phi\phi \rightarrow \phi\phi$  and  $\psi\psi \rightarrow \psi\psi$  channels, which have not been considered in the existing literature.

The rest of the paper is organized as follows. In Sec. 2 we present an effective coupling analysis of a singlet scalar coupled to VLFs. In Sec. 2.1 we present the LHC gluon-gluon fusion rate and the diphoton rate  $\sigma(pp \rightarrow \gamma\gamma)$  as a function of the  $\phi gg$  and  $\phi\gamma\gamma$  effective couplings for different total  $\phi$  widths. In Sec. 2.2 and Sec. 2.3 we discuss the LHC constraints and perturbative unitarity constraints respectively. In Sec. 3 we analyze a gauge-singlet vector-like fermion dark matter model, show regions of parameter space that give the observed dark matter relic density and are consistent with dark matter direct-detection experiment and perturbative unitarity constraints, and show the  $\sigma(pp \rightarrow \gamma\gamma)$  cross section at the LHC. In Sec. 4 we offer our conclusions, and point out some promising signals to look for at the LHC to ascertain if this model is realized in nature. In App. A we collect the formulas for the fermion contributions to the gluon-gluon-scalar ( $\phi gg$ ) and gamma-gamma-scalar ( $\phi\gamma\gamma$ ) couplings. In App. B we present the relevant formulas for the dark matter relic density calculation in the singlet scalar model.

## 2 Effective coupling analysis

In this section we present a model-independent analysis of new vector-like fermions coupled to a gauge-singlet scalar and to SM fermions. Our goal is to obtain in terms of the effective couplings, the 13 TeV LHC  $\sigma(pp \rightarrow \phi \rightarrow \gamma\gamma)$  and the possible constraints from the 8 TeV and 13 TeV LHC. We also determine the constraints on the  $\phi$  Yukawa couplings from perturbative unitarity. We assume that the new scalar is produced via gluon fusion process as it is usually the dominant process. We

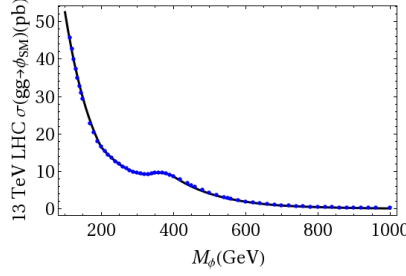


Figure 1: The solid curve shows the 13 TeV  $\sigma(gg \rightarrow \phi)$  (in pb) obtained by using fitting functions on the values obtained from Ref. [20], which are shown as blue dots.

start by effectively parameterizing the relevant interactions as

$$\mathcal{L} \supset -\frac{y_\psi}{\sqrt{2}}\phi\bar{\psi}\psi - \frac{y_{ff}}{\sqrt{2}}\phi\bar{f}f - \frac{\kappa_{\phi hh}M_\phi}{2\sqrt{2}}\phi h^2 - \frac{y_f}{\sqrt{2}}\bar{f}_L H f_R + h.c. , \quad (1)$$

where  $H$  denotes the SM Higgs doublet containing the physical Higgs boson  $h$  with  $m_h = 125$  GeV,  $\phi$  denotes the new scalar,  $\psi$  denotes new VLFs, and  $f$  denotes SM fermions (SMF). In the model of Sec. 3 many of these operators are generated and we draw from the analysis performed here to infer the implications for that model.

In terms of the couplings defined in Eq. (1), the effective  $\phi gg$  and  $\phi\gamma\gamma$  couplings,  $\kappa_{\phi gg}$  and  $\kappa_{\phi\gamma\gamma}$  are given in App. A. The  $\kappa_{\phi hh}$  term leads to the  $\phi \rightarrow hh$  decay, which as we see below is constrained at the LHC. We find that the  $\kappa_{\phi hh}$  contributes to  $\kappa_F^2$  an amount  $(\kappa_{\phi hh}^2/4)\sqrt{1 - 4m_h^2/M_\phi^2}$ .

## 2.1 Gluon-gluon fusion and diphoton rate

Here we show the LHC diphoton rate as a function of the  $\phi gg$  and  $\phi\gamma\gamma$  effective couplings. We work in the narrow width approximation (NWA) in which we can write  $\sigma(pp \rightarrow \phi \rightarrow \gamma\gamma) \approx \sigma(pp \rightarrow \phi) * BR(\phi \rightarrow \gamma\gamma) \equiv \sigma_\phi * BR_{\gamma\gamma}$  with  $BR(\phi \rightarrow \gamma\gamma) \equiv \Gamma(\phi \rightarrow \gamma\gamma)/\Gamma_\phi$  where  $\Gamma_\phi$  is the total width of the  $\phi$ . We consider here  $\phi$  production via the gluon-fusion channel. Rather than compute  $\sigma(gg \rightarrow \phi)$  ourselves, we relate it to the SM-like Higgs production c.s. at this mass and make use of the vast literature on this by writing

$$\sigma(gg \rightarrow \phi) = \sigma(gg \rightarrow \phi_{\text{SM}}) \frac{\Gamma(\phi \rightarrow gg)}{\Gamma(\phi_{\text{SM}} \rightarrow gg)} , \quad (2)$$

where  $\phi_{\text{SM}}$  denotes a scalar with SM-Higgs-like couplings to other SM states with the mass taken as a free parameter. We take from Ref. [20] the 14 TeV LHC  $\sigma(\phi_{\text{SM}} \rightarrow gg)$  for  $M_{\phi_{\text{SM}}}$  up to 1000 GeV and multiply by 0.9 to get the  $\sqrt{s} = 13$  TeV values [21]. To obtain the LHC  $\sigma(gg \rightarrow \phi_{\text{SM}})$  values for arbitrary  $M_\phi$ , we interpolate the values given in Ref. [20] using well chosen fitting functions, and the resulting fit is shown in Fig. 1 as the solid line, while the values obtained from Ref. [20] are shown by the blue dots. As can be inferred from Eq. (2) and detailed in Ref. [22], a colored fermion (quark) coupled to  $\phi$  via a Yukawa coupling  $y'_f/\sqrt{2}$ , gives a contribution to  $\sigma(gg \rightarrow \phi)$  given by

$$\sigma(gg \rightarrow \phi) = \sigma(gg \rightarrow \phi_{\text{SM}}) \left| \sum_f \frac{y_f}{\hat{y}_t} \frac{F_{1/2}(\tau_f)}{F_{1/2}(\tau_t)} \frac{m_t}{M_f} \right|^2 , \quad (3)$$

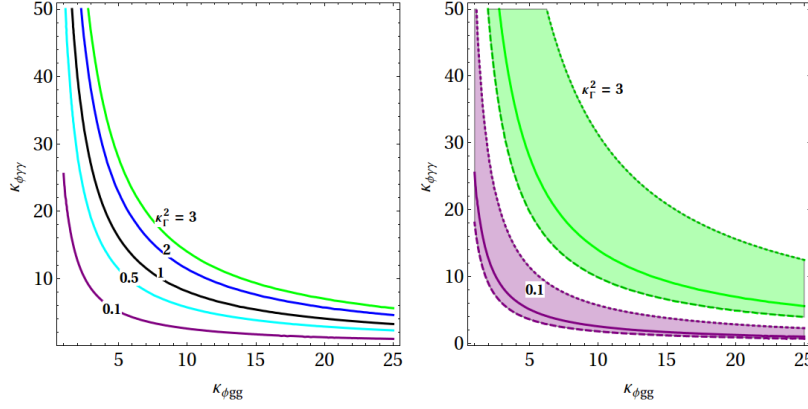


Figure 2: For various  $\kappa_\Gamma^2$  shown, the  $\kappa_{\phi gg}$  and  $\kappa_{\phi\gamma\gamma}$  that leads to  $\sigma_\phi * BR_{\gamma\gamma} = 1$  fb (left), and the regions  $0.5 \leq \sigma_\phi * BR_{\gamma\gamma} \leq 5$  fb around  $\kappa_\Gamma^2 = 3$  (green), 0.1 (purple) curves (right) with  $M_\phi = 1000$  GeV.

where  $\hat{y}_t = \sqrt{2}m_t/v$  is the  $\hat{h}tt$  Yukawa coupling,  $\tau_f \equiv M_\phi^2/(4m_f^2)$ , and  $F_{1/2}$  is defined in App. A. Here  $\hat{h}$  is the interaction basis SM-Higgs which after taking into account a possible mixing with the  $\phi$  will be identified as the 125 GeV Higgs. The sum over  $f$  in the numerator includes the top-quark contribution.

We define the parameter  $\kappa_\Gamma^2 = 16\pi\Gamma_\phi/M_\phi$  and write the  $\phi$  width ( $\Gamma_\phi$ ) as

$$\Gamma_\phi \equiv \frac{\kappa_\Gamma^2}{16\pi} M_\phi. \quad (4)$$

The  $\kappa_\Gamma^2$  includes all couplings relevant to  $\phi$  decay, and phase-space factors as appropriate. For example, for the decay into colored fermions much lighter than  $M_\phi$ , coupled via a Yukawa coupling  $y_0/\sqrt{2}$ , we have  $\kappa_\Gamma^2 = N_c y_0^2$ . From Eqs. (2) and (4), the LHC  $\sigma_\phi * BR(\phi \rightarrow \gamma\gamma)$  in terms of the effective couplings can be written as

$$\sigma_\phi * BR_{\gamma\gamma} = \left[ \sigma(gg \rightarrow \phi_{\text{SM}}) \frac{\kappa_{\phi gg}^2}{\kappa_{hgg}^2} \right] * \left[ \frac{1}{4} \left( \frac{\kappa_{\phi\gamma\gamma}}{16\pi^2 M} \right)^2 \frac{M_\phi^2}{\kappa_\Gamma^2} \right], \quad (5)$$

where  $M$  is a reference mass-scale which we set to 1 TeV. Expression for the  $\Gamma(\phi \rightarrow XX)$  can be found for example in Refs. [22, 23]. In Fig. 2 we show for various  $\kappa_\Gamma^2$  the  $\kappa_{\phi gg}$  and  $\kappa_{\phi\gamma\gamma}$  required for  $\sigma_\phi * BR_{\gamma\gamma} = 1$  fb with the benchmark point  $M_\phi = 1000$  GeV. We also show in Fig. 2 a band around  $\kappa_\Gamma^2 = 3, 0.1$ , three representative total width values. The diphoton rate is presented for a CP-even scalar and the CP-odd scalar rate will be different due to  $\mathcal{O}(1)$  factor differences in the  $\phi gg$  and  $\phi\gamma\gamma$  loop factors.

## 2.2 LHC constraints

If the  $\phi t\bar{t}$  and  $\phi \tau\bar{\tau}$  couplings are nonzero,  $\phi$  decays to  $t\bar{t}$  and  $\tau\bar{\tau}$  also. Since there are no reported excesses in these channels, there could be nontrivial constraints on the models from these channels. We discuss these constraints next.

In Ref. [22] Fig. 2, we show constraints on the  $\kappa_{\phi gg}$  from the 8 TeV LHC exclusion limits. To summarize this, for  $BR_{t\bar{t}} = 1$ , the constraint from the  $t\bar{t}$  channel is  $\kappa_{\phi gg} < 26$ , and for  $BR_{\tau\bar{\tau}} = 1$ , the constraint from the  $\tau\bar{\tau}$  channel is  $\kappa_{\phi gg} < 4$ . Of course, in a particular model, these BRs can

be significantly smaller than 1, particularly  $BR_{\tau\tau}$ , and the limits can be correspondingly weaker. For example a SM-like theory with only the Higgs mass set at 1000 GeV, we have  $\kappa_{\phi_{\text{SM}}gg} = 7$  with  $\sigma(pp \rightarrow \phi_{\text{SM}}) \approx 30$  fb at the 8 TeV LHC due mainly to the top contribution. From the  $\kappa_{\phi gg}$  expressions in Eq. (B.1) of Ref. [22] and with  $BR_i = \kappa_i^2/\kappa_{\Gamma}^2$ , we derive the bound

$$\left| \sum_Q \frac{y_{\phi QQ}}{\hat{y}_t} \frac{F_{1/2}(\tau_Q)}{F_{1/2}(\tau_t)} \frac{m_t}{M_Q} \right|^2 \frac{\kappa_i^2}{\kappa_{\Gamma}^2} < \left( \frac{\kappa_{\phi gg(i)}^{\text{max}}}{\kappa_{\phi_{\text{SM}}gg}} \right)^2, \quad (6)$$

where the sum over  $Q$  includes the top-quark contribution plus any new colored vector-like fermions present in the  $\phi gg$  loop,  $\hat{y}_t \approx 1$  is the SM top Yukawa coupling (we ignore the effect of running this to the scale  $\mu = M_{\phi}$ ), and  $\kappa_t^2 = N_c y_{\phi tt}^2 (1 - 4r_t)^{n/2}$ ,  $\kappa_{\tau}^2 = y_{\phi \tau\tau}^2 (1 - 4r_{\tau})^{n/2}$  with  $n = 3$  for a CP-even  $\phi$  and  $n = 1$  for a CP-odd  $\phi$ , and  $r_f \equiv M_f^2/M_{\phi}^2$ . The index  $(i)$  runs over various channels  $\{t\bar{t}, \tau\bar{\tau}, hh, gg, \dots\}$  i.e.  $(i) = \{t, \tau, h, g\}$ , and we have  $\kappa_{\phi gg(t)}^{\text{max}} = 20$ ,  $\kappa_{\phi gg(\tau)}^{\text{max}} = 4$  (corresponding to  $BR_i = 1$ ) as derived in Ref. [22]. The LHC upper limit on the  $hh$  channel  $\sigma * BR$  at a mass of 1000 GeV is about 10 fb [19], which translates into  $\kappa_{\phi gg(h)}^{\text{max}} = 4$ . The LHC upper limit on the dijet channel at a mass of 1000 GeV is about 30 pb [24], and for the sizes of cross-section and dijet BR we are dealing with here, this will not be a nontrivial constraint.

Generically, in new physics models there are shifts in the  $h$  couplings to SM states, which are constrained by the LHC data (see for example Ref. [25]). In the model we consider below, the  $hh$  channel constraint quoted above is particularly constraining and requires the Higgs-singlet mixing to be small ( $\lesssim 0.05$ ), and once this is ensured, the constraints from the Higgs coupling measurements are satisfied. In the model we discuss below, vector-like fermions are present, and there are direct LHC limits on them that have to be obeyed. Preventing a stable cosmological colored relic implies that they have to be allowed to mix with SM fermions. Allowing only mixing to third generation SM quarks is sufficient and is relatively safer with respect to FCNC constraints. We assume that there are small off diagonal mass mixing terms  $\delta m$  to third-generation quarks such that  $\delta m/M_{VL} \lesssim 0.1$  to third generation SM quarks but big enough such that the VLQ decays such that it is not in conflict with cosmological data. We summarize next the present LHC lower limits on VLF masses, with the precise limit depending on the BRs. The lower limit on the  $t'$  mass is presently in the range 1000 – 920 GeV [26, 27, 28, 29, 30], and on the  $b'$  mass in the range 740 – 900 GeV [30, 31, 32]. For a long-lived VLQ with life-times in the range  $10^{-7} - 10^5$  s, the bound is looser with  $M_Q \gtrsim 525$  GeV being allowed [33, 34].<sup>1</sup> The lower limit on VLL masses is presently  $\lesssim 100$  GeV if it decays only into a  $\tau$ , and about 300 GeV (450 GeV) for a singlet (doublet) that decays into  $e, \mu$  [36].

## 2.3 Unitarity constraint

If the  $\phi\psi\psi$  coupling becomes too large then certain processes will violate the perturbative unitarity. Here we obtain the constraints on the  $\phi\psi\psi$  couplings from the perturbative unitarity of  $\psi\psi \rightarrow \psi\psi$  and  $\phi\phi \rightarrow \phi\phi$  process. The tree level contribution leads to a very loose bound, and we therefore consider the 1-loop box diagram shown in Fig. 3. Expanding the amplitude  $\mathcal{M}$  in partial waves as

<sup>1</sup> It may be possible to weaken the VLQ mass bound somewhat by allowing  $t' \rightarrow t\phi'$  and/or  $b' \rightarrow b\phi'$  decays, where  $\phi'$  is an SU(2) singlet and will lead to missing energy at the LHC. This for example can be achieved by introducing the operators  $U\phi't^c$  or  $B\phi'b^c$  where the  $U$  and  $B$  are the charge 2/3 and  $-1/3$  SU(2) singlet VLFs,  $t^c$  and  $b^c$  are SM SU(2) singlet fermions. Due to the new decay mode, the usual assumption that the BRs into the SM final states ( $bW, tZ, t\bar{t}$  for the  $t'$  for instance) sum to one fails, and the limits have to be reanalyzed. The BRs into the SM final states are decreased and since the new mode has substantially larger SM irreducible SM  $t\bar{t} + \cancel{E}_T$  (or  $b\bar{b} + \cancel{E}_T$ ) backgrounds, the VLQ lower limits should be weaker. A detailed investigation of the implications of this proposal is beyond the scope of this work. For instance, the model discussed in Ref. [35] has this possibility.

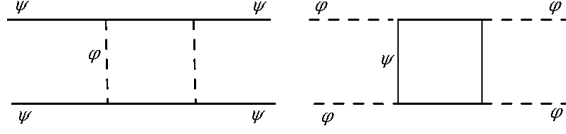


Figure 3: 1-loop box diagrams contributing to  $\psi\psi \rightarrow \psi\psi$  (left) and  $\phi\phi \rightarrow \phi\phi$  (right) processes.

$$\mathcal{M}(\cos \theta) = 16\pi \sum_l (2l+1) a_l P_l(\cos \theta) , \quad (7)$$

a necessary condition for unitarity is  $\text{Im } a_l \leq 1$  [37]. Using the optical theorem, we can compute the  $\text{Im}(\mathcal{M}(\psi\psi \rightarrow \psi\psi))$  for forward scattering in terms of the cross section  $\sigma(\psi\psi \rightarrow \phi\phi)$  with the precise relation given by (see for example Ref. [38])

$$\text{Im} \{ \mathcal{M}(\psi(p_1)\psi(p_2) \rightarrow \psi(p_1)\psi(p_2)) \} = 2E_{cm} p_{cm} \sigma(\psi(p_1)\psi(p_2) \rightarrow \phi(k_1)\phi(k_2)) . \quad (8)$$

For  $\sigma$  we compute the spin-averaged cross section for  $\psi\psi \rightarrow \phi\phi$  scattering as

$$\frac{d\sigma}{d\cos\theta} = \frac{y_\psi^4}{128\pi s} \tilde{f}(\cos\theta) , \quad \text{where } \tilde{f}(\cos\theta) = \frac{(1-2r_{\phi E})^{3/2}(1-\cos^2\theta)}{2(1-r_{\phi E}-\sqrt{1-2r_{\phi E}\cos\theta})^2} , \quad (9)$$

where we have ignored the fermion mass, and  $r_{\phi E} \equiv M_\phi^2/(2E_\psi^2)$ . Integrating this over  $\cos\theta \in (-1, 1)$ , we obtain for  $E_\psi \gtrsim M_\phi$  the approximate equality  $\sigma(\psi\psi \rightarrow \phi\phi) \approx y_\psi^4/(128\pi s)$ . To get a conservative bound, we assume that the  $\psi\psi \rightarrow \psi\psi$  amplitude is saturated by the  $l=0$  partial-wave, and obtain  $\text{Im } a_0 = y_\psi^4/(4 \times (16\pi)^2) < 1$ , i.e.  $y_\psi < 10$  as the unitarity bound. The related process  $\phi\phi \rightarrow \phi\phi$  also leads to a similar bound, but the amplitude is enhanced by  $N_c$  for a colored fermion in the 1-loop amplitude of Fig. 3, and leads to a bound  $\sum_f y_f (N_c^f)^{1/4} \lesssim 10$  where  $N_c^f = 3$  for a colored fermion (and  $N_c^f = 1$  for an uncolored fermion), and the sum is over all fermions that contribute in the loop.

### 3 Vector-Like fermion dark matter model and phenomenology

In this section we analyze a SM gauge-singlet vector-like fermion dark matter candidate coupled to a CP-even singlet scalar  $\phi$ , which is also coupled to a vector-like quark. A coupling between the vector-like fermionic dark matter  $\psi$  and the SM sector can arise via the Higgs-portal due to a mixing between the  $\phi$  and the SM Higgs boson. This mixing is possible only for a CP-even scalar if  $CP$ -invariance is not to be broken spontaneously.

We introduce an  $SU(2)_L \times U(1)_Y$  singlet VLF  $\psi$  with mass  $M_\psi$ , along with an  $SU(2)$ -singlet scalar  $\hat{\phi}$ , and an  $SU(2)$ -singlet color-triplet VLQ  $U$  with hypercharge  $Y_U$  and mass  $M_U$ . This model and the couplings to the VLF parallels the SVU model of Ref. [22], and in the notation of that paper we refer to this model as the  $SVU\psi$  model. We write an effective Lagrangian

$$\mathcal{L} \supset M_h^2 H^\dagger H + M_\phi^2 \Phi^\dagger \Phi - \kappa \Phi^\dagger \Phi H^\dagger H - \frac{\mu}{\sqrt{2}} \hat{\phi} H^\dagger H - M_\psi \bar{\psi} \psi - M_U \bar{U} U - \frac{y_\psi}{\sqrt{2}} \hat{\phi} \bar{\psi} \psi - \frac{y_U}{\sqrt{2}} \hat{\phi} \bar{U} U , \quad (10)$$

where we show only the relevant terms and do not repeat the SM terms. We assume that the potential is such that  $\langle \Phi \rangle = \xi/\sqrt{2}$  and  $\langle H \rangle = v/\sqrt{2}$ , and denote the fluctuations around these as  $\hat{\phi}$

and  $\hat{h}$  respectively. The effective coupling  $\kappa_{\phi hh}$  defined in Eq. (1) is given as  $\kappa_{\phi hh} = \sqrt{2}(\mu + \kappa\xi)/M_\phi$ . The  $\hat{\phi}$  and  $\hat{h}$  mix after EWSB and the mixing angle  $\sin\theta_h \equiv s_h$  is given by

$$\tan(2\theta_h) = \frac{\sqrt{2}\kappa_{\phi hh}}{\left(1 - M_h^2/M_\phi^2\right)} \frac{v}{M_\phi}, \quad (11)$$

with the effective coupling  $\kappa_{\phi hh}$  defined in Eq. (10). Diagonalizing the  $\hat{\phi} \leftrightarrow \hat{h}$  mixing terms, we go from the  $(\hat{h}, \hat{\phi})$  basis to the mass basis  $(h, \phi)$ , and define the mass eigenstates to be  $h = c_h \hat{h} - s_h \hat{\phi}$  and  $\phi = s_h \hat{h} + c_h \hat{\phi}$ . In the  $(\phi, h)$  mass basis we have

$$\mathcal{L}_{\phi hh} = -\frac{1}{4} \tan 2\theta_h (c_h^3 - 2c_h s_h^2) \frac{(M_\phi^2 - M_h^2)}{v} \phi h h. \quad (12)$$

In our numerical analysis below, we treat  $s_h$  as an input parameter, and one can always relate it to the  $\mathcal{L}$  parameters in a model if needed using Eq. (11). In order to agree with the Higgs observables already measured at the LHC,  $s_h$  must be small as we show later. The phenomenology of the  $\kappa$  is discussed in detail for example in Ref. [7]. For example, for  $s_h = 0.01$ , we have  $\kappa_{\phi hh} = 0.04$ .

Mixed operators such as

$$\mathcal{L}_{\text{mix}} \supset -\tilde{y}_U \bar{U} q_L^3 \cdot H - \tilde{y}_\psi \bar{\psi} \ell_L^3 \cdot H + \text{h.c.}, \quad (13)$$

are allowed if  $Y_U = 2/3$  and where  $q_L^3$  is the third-generation SM quark doublet, and  $\ell_L^3$  is the third-generation SM lepton doublet. To be safe from FCNC constraints, we allow couplings with only third-generation SM fermions. To prevent having a cosmologically stable  $U$ , we take  $\tilde{y}_U$  to be small enough that all FCNC constraints are obeyed, but big enough that  $U$  decays promptly to SM final states as discussed in detail in Ref. [39], and we do not therefore discuss further the consequences of this operator in this work. The  $\mathcal{L}$  respects a  $Z_2$  symmetry under which  $\psi \rightarrow -\psi$ , and this  $Z_2$  symmetry is broken only by the  $\tilde{y}_\psi$  term. Thus, if  $\tilde{y}_\psi = 0$ , the  $\psi$  is absolutely stable and is a possible dark matter candidate. One then has to ensure that the parameters are chosen in such a way that the relic density is not so high that it over-closes the universe, or the direct-detection cross-section is not so high that it is excluded by experiment. We explore this possibility in detail below.

The  $\sigma_\phi * BR_{\gamma\gamma}$  can be obtained from Eq. (5), and the expressions for  $\kappa_{\phi gg}$  and  $\kappa_{\phi\gamma\gamma}$  are given in App. B of Ref. [22]. In  $\Gamma_\phi$  we include the partial widths  $\Gamma(\phi \rightarrow \psi\psi, hh, tt, gg)$ . In Fig. 4 we show  $\sigma_\phi * BR_{\gamma\gamma}$  vs.  $\kappa_\Gamma^2$  in the model, for  $M_\psi = 475$  GeV,  $M_U = 1200$  and  $1500$  GeV,  $M_\phi = 1000$  GeV,  $Y_U = 2/3$ ,  $s_h = 0.01$  and scanning over  $y_U, y_\psi$  in the range  $0 < y_U < y_U^{\text{max}}$ ,  $0 < y_\psi < y_\psi^{\text{max}}$ , subject to the unitarity constraint  $y_\psi + y_U N_c^{1/4} < 10$  computed in Sec. 2.3. The 8 TeV  $hh$  channel constraints discussed in Sec. 2.2 constrains  $\kappa_{\phi hh} \ll 1$ . For instance this implies the bound  $s_h \lesssim 0.07$  for  $y_U = 5$  and  $\kappa_\Gamma^2 = 0.4$ . For  $y_\psi \gtrsim 0.1$ , the  $BR(\phi \rightarrow \psi\psi)$  is dominant and  $y_\psi$  largely controls  $\kappa_\Gamma^2$ . For  $\kappa_\Gamma^2 = 1$ , the  $\sigma_\phi * BR_{\gamma\gamma}$  can reach only 0.03 fb for  $s_h = 0.01$  as seen in Fig. 4. For very small  $y_\psi \lesssim 0.1$ , the total width (i.e.  $\kappa_\Gamma^2$ ) is small and dominated by top and  $U$  loops and the tree-level  $\phi \rightarrow hh, tt$  decays. For  $y_\psi \rightarrow 0$ ,  $s_h \rightarrow 0$  both  $\sigma * BR_{\gamma\gamma}$  and  $\kappa_\Gamma^2$  comes from  $U$  loops and scales as  $y_U^4$  and  $y_U^2$  respectively;  $\sigma * BR_{\gamma\gamma}$  increases with  $\kappa_\Gamma^2$  in this region up to around  $\kappa_\Gamma^2 \simeq 0.03$  as can be seen from Fig. 4. We can see that for  $s_h = 0.01$  we can get  $\sigma * BR_{\gamma\gamma} \simeq 5$  fb.

In Fig. 5 we show contours of  $\sigma_\phi * BR_{\gamma\gamma}$  (in fb), and various  $\kappa_\Gamma^2$  as colored regions, with the parameters not along the axes fixed at  $s_h = 0.01$ ,  $M_\psi = 475$  GeV,  $M_U = 1200$  GeV,  $M_\phi = 1000$  GeV  $y_\psi = 1$ ,  $y_U = 5$ . We also show in Fig. 5 the unitarity constraint on  $y_\psi$  (shown here by red line) for  $y_U = 5$ . For  $y_U = 5$ ,  $\sigma_\phi \simeq 0.6$  pb and The partial widths  $\Gamma_{\{hh, tt, gg\}}$  for  $s_h = 0.01$ ,  $M_U = 1000$  GeV



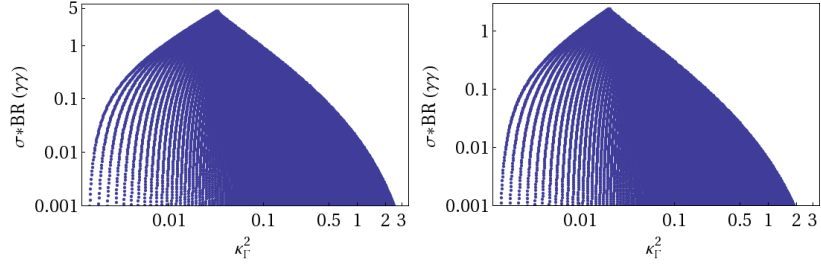


Figure 4: For  $Y_U = 2/3$ , the  $\sigma_\phi * BR_{\gamma\gamma}$  (in fb) vs.  $\kappa_\Gamma^2$ , for  $M_\psi = 475$  GeV,  $M_U = 1200$  (left) and 1500 GeV (right),  $M_\phi = 1000$  GeV,  $s_h = 0.01$  and  $y_U, y_\psi$  scanned over the range  $0 < y_U < y_U^{max}$ ,  $0 < y_\psi < y_\psi^{max}$  subject to the unitarity constraint.

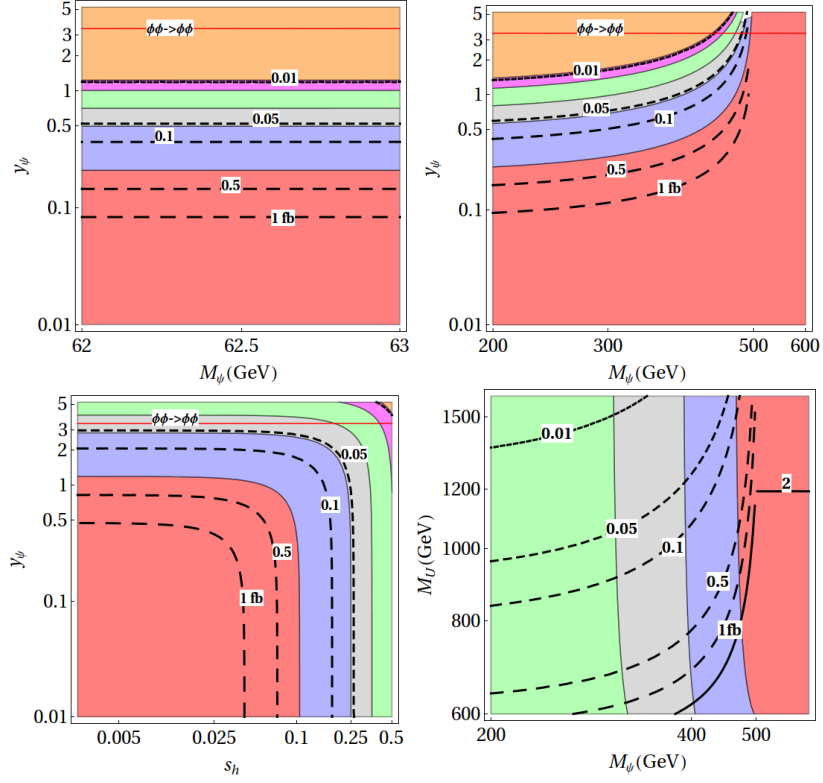


Figure 5: For  $Y_U = 2/3$ , the contours of  $\sigma_\phi * BR_{\gamma\gamma}$  (in fb), and regions of  $\kappa_\Gamma^2 < 0.1$  (red),  $0.1 < \kappa_\Gamma^2 < 0.5$  (blue),  $0.5 < \kappa_\Gamma^2 < 1$  (gray),  $1 < \kappa_\Gamma^2 < 2$  (green),  $2 < \kappa_\Gamma^2 < 3$  (pink),  $\kappa_\Gamma^2 > 3$  (orange); parameters not along the axes are fixed at  $s_h = 0.01$ ,  $M_\psi = 475$  GeV,  $M_U = 1200$  GeV,  $M_\phi = 1000$  GeV  $y_\psi = 1$ ,  $y_U = 5$ . Unitarity constraint on  $y_\psi$  for  $y_U = 5$  is shown by the red horizontal line.



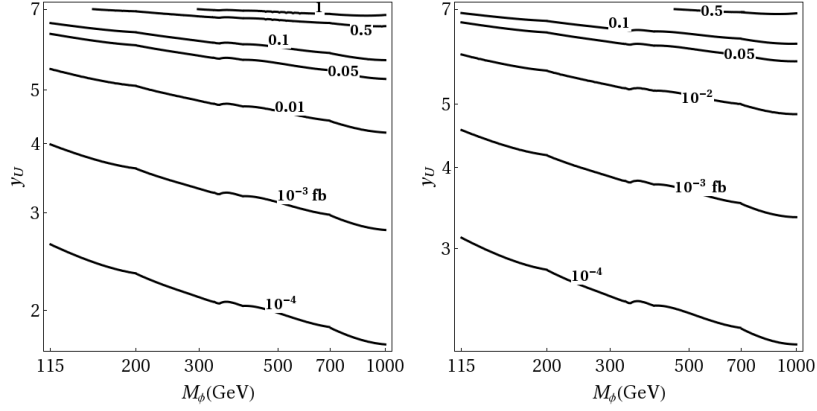


Figure 6: Contours of  $\sigma(\phi) * BR(\gamma\gamma)$  (in fb) for  $M_U = 1200$  GeV (left),  $M_U = 1500$  GeV (right) with  $M_\psi = M_\phi/2 - 25$  GeV,  $s_h = 0.01$  and  $y_\psi$  chosen to saturate the unitarity constraint  $y_U N_c^{1/4} + y_\psi \leq 10$ .

are 0.015, 0.004, 0.27 GeV respectively. For very small  $y_\psi$  or  $M_\psi > M_\phi/2$ ,  $\Gamma(\phi \rightarrow \psi\psi) \simeq 0$  and  $\Gamma_\phi$  is dominated by  $\Gamma_{\{hh, tt, gg\}}$ ; in this limit  $BR_{\gamma\gamma} \simeq 3.3 * 10^{-3}$  and  $\sigma * BR_\gamma \simeq 1.8$  fb for the set of parameters chosen with  $s_h = 0.01$ . For  $M_\psi < M_\phi/2$  and  $y_\psi$  large,  $\Gamma_\phi$  is large being dominated by  $\phi \rightarrow \psi\psi$  decay resulting in very small  $\sigma * BR_{\gamma\gamma}$ . In Fig. 6 we show the contours of  $\sigma(\phi) * BR(\gamma\gamma)$  (in fb) for  $s_h = 0.01$ ,  $M_U = 1200$  and 1500 GeV,  $M_\phi = 1000$  GeV,  $M_\psi = M_\phi/2 - 25$  GeV with  $y_\psi$  chosen to satisfy the unitarity constraints  $y_U N_c^{1/4} + y_\psi \leq 10$ .

In the region where  $M_\psi$  is within about 5 MeV of  $M_\phi/2$  and if  $\Gamma_\psi < 0.1$  MeV, a large threshold enhancement is possible [40], which we do not include in our analysis.

If  $\tilde{y}_\psi$  of Eq. (13) is zero, the  $Z_2$  symmetry is exact,  $\psi$  is stable and can potentially be a dark matter candidate. The dark matter relic density and direct-detection can be computed as detailed, for example, in Ref. [7] and App. A of Ref. [39]. In order to get the correct relic density of  $\Omega_{dm} = 0.26 \pm 0.015$  [41], we need the thermally averaged self-annihilation cross-section to be  $\langle\sigma v\rangle \approx 2.3 \times 10^{-9}$  GeV $^{-2}$ . We have for our case [7, 39]

$$\langle\sigma v\rangle = \frac{6}{x_f} \frac{1}{8\pi s} \sum_i |\mathcal{B}_i|^2 \hat{\Pi}_{PS}^i, \quad (14)$$

where  $x_f \equiv M_\psi/T_f \approx 25$  with  $T_f$  the freeze-out temperature, the sum is over all self-annihilation processes  $\psi\psi \rightarrow f_i f_i$  for final states  $f_i$  kinematically allowed, the  $|\mathcal{B}_i|^2$  is the coefficient of  $v_{rel}^2$  in the amplitude squared for each process,  $v_{rel}$  being the relative velocity of the two initial state  $\psi$ ; the  $\hat{\Pi}_{PS}^i \equiv \sqrt{(1 - 4m_i^2/s)}$  is a phase-space factor with  $m_i$  the mass of the final-state particle, and  $s$  is the Mandelstam variable, which for a cold-dark matter candidate during freeze-out is  $s \approx 4M_\psi^2$ . In our analysis we include the two-body final states  $b\bar{b}, WW, ZZ, hh, t\bar{t}, gg$ , whichever are kinematically allowed for that given  $M_\psi$ . Although  $\tau\tau$  and  $\gamma\gamma$  final states are also possible, we ignore them in our analysis as these contributions are small. For large  $s_h$ , the loop level  $gg$  contribution is small compared to other tree level contribution. But for small  $s_h$ ,  $gg$  contribution becomes comparable or even larger than the tree level processes. Details of the  $\mathcal{B}_i$  for each of these final states are given in Appendix B.

The dark-matter direct-detection elastic scattering cross-section on a nucleon is mediated by scalar exchange. Since  $h$  is lighter than  $\phi$ , the former mostly contributes, but if  $s_h \lesssim 0.05$ , the

latter's contribution is also important. The  $h$  exchange contribution is given for example in Ref. [7], which we generalize here to include  $\phi$  contribution also since we consider  $s_h \lesssim 0.05$ . The scalar-nucleon-nucleon coupling is generated due to the scalar coupling to the quark content of the nucleon, and also due the scalar coupling to the gluon content of the nucleon via the  $ggh, gg\phi$  effective couplings. We define an effective Lagrangian for the scalar-nucleon-nucleon interaction as

$$\begin{aligned}\mathcal{L} &\supset \lambda_{hNN} \hat{h} \bar{N} N + \lambda_{\phi NN} \hat{\phi} \bar{N} N, \\ &= (c_h \lambda_{hNN} - s_h \lambda_{\phi NN}) h \bar{N} N + (c_h \lambda_{\phi NN} + s_h \lambda_{hNN}) \phi \bar{N} N,\end{aligned}\quad (15)$$

where  $N$  denotes the nucleon, and in the second line we write in the mass basis. We take  $\lambda_{hNN} = 2 \times 10^{-3}$  [42, 43], but recent updates indicate a smaller value of  $\lambda_{hNN} \approx 1.1 \times 10^{-3}$  [44]. We derive  $\lambda_{\phi NN}$  using the formalism and notation of App. C of Ref. [43], to get the singlet VLQ (up-type  $U$ ) contribution to the  $\phi NN$  coupling via its contribution to the  $\phi gg$  couplings, and the gluon content of the nucleon, which leads us to  $\lambda_{\phi NN} = (2/27) f_{TG}^{(p,n)} y_U m_{(p,n)} / M_U \approx 0.063 y_U m_N / M_U$ . We can now write the  $\psi$  elastic scattering cross section on a nucleon for  $q^2 \ll m_N^2$  as

$$\begin{aligned}\sigma(\psi N \rightarrow \psi N) &= \frac{y_\psi^2}{8\pi} \left[ \frac{s_h(c_h \lambda_{hNN} - s_h \lambda_{\phi NN})}{M_h^2} - \frac{c_h(c_h \lambda_{\phi NN} + s_h \lambda_{hNN})}{M_\phi^2} \right]^2 (|\mathbf{p}_\psi|^2 + m_N^2), \\ &= \frac{y_\psi^2 s_h^2 c_h^2 \lambda_{hNN}^2 (|\mathbf{p}_\psi|^2 + m_N^2)}{8\pi M_h^4} \left[ 1 - \frac{\lambda_{\phi NN} c_h (1 + \Delta_\phi)}{\lambda_{hNN} s_h (1 - \Delta_h)} \frac{M_h^2}{M_\phi^2} \right]^2,\end{aligned}\quad (16)$$

where  $p_\psi \approx M_\psi v_\psi$  with  $v_\psi \sim 10^{-3}$  [43],  $m_N \approx 1$  GeV is the nucleon mass,  $\Delta_h = (\lambda_{\phi NN} / \lambda_{hNN})(s_h / c_h)$ , and  $\Delta_\phi = (\lambda_{hNN} / \lambda_{\phi NN})(s_h / c_h)$ . This is the generalization of the direct-detection elastic cross section Eq. (13) of Ref. [7] which included only the  $h$  contribution, to now include the  $\phi$  contribution also that becomes important for very small  $s_h$ .<sup>2</sup> There is also uncertainty on the local dark matter halo density and its velocity distribution (for a discussion of these uncertainties, see for example Refs. [45]). Given these uncertainties, our direct-detection rates should be taken to be accurate only up to unknown  $\mathcal{O}(1)$  factors.

In Fig. 7 we plot contours of  $\Omega_{dm} = 0.1, 0.25, 0.3$  and for  $M_\phi = 1000$  GeV  $\lambda_N = 2 \times 10^{-3}$ ,  $m_N = 1$  GeV, show the regions with  $\sigma_{DD} > 5 \times 10^{-45} \text{ cm}^2$ ,  $10^{-45} \text{ cm}^2 < \sigma_{DD} < 5 \times 10^{-45} \text{ cm}^2$ ,  $10^{-46} \text{ cm}^2 < \sigma_{DD} < 10^{-45} \text{ cm}^2$ ,  $10^{-47} \text{ cm}^2 < \sigma_{DD} < 10^{-46} \text{ cm}^2$ ,  $10^{-48} \text{ cm}^2 < \sigma_{DD} < 10^{-47} \text{ cm}^2$ ,  $10^{-49} \text{ cm}^2 < \sigma_{DD} < 10^{-48} \text{ cm}^2$ ,  $\sigma_{DD} < 10^{-49} \text{ cm}^2$  with parameters not varied along the axes fixed at  $s_h = 0.01$ ,  $M_\psi = 475$  GeV,  $y_U = 5$  and  $M_U = 1200$  GeV.  $M_\phi = 1200$  GeV. We also show in Fig. 7 the unitarity constraint on  $y_\psi$  from  $\phi\phi \rightarrow \phi\phi$  process for  $y_U = 5$ . We see that for  $s_h = 0.01$ ,  $y_\psi \leq 3$  the direct-detection cross section is close to or less than the current experimental limit  $\sigma_{DD} \leq (0.1 - 1) \times 10^{-45} \text{ cm}^2$  [46] for dark matter mass in the 10 – 1000 GeV range. The correct self-annihilation cross-section is obtained only with an enhancement of the cross-section at the  $\phi, h$  pole with  $M_\psi \sim M_{\phi,h}/2$ . Being close to the  $\phi$  pole suppresses the  $\phi \rightarrow \psi\psi$  decay rate due to the limited phase-space available, leading to a small  $\kappa_\Gamma^2 \ll 0.1$  as can be seen from Fig. 5. Since we are required to have  $s_h \ll 1$  in which case the  $gg$  contribution dominates, the dark matter relic-density scales as  $\sim (y_\psi y_U)^{-2}$  to a very good approximation as can be inferred from Eqs. (14) and (B.18). Similarly, the dark matter direct-detection rate also scales the same way in this limit, as evident from Eq.(16). Thus, for  $M_\phi = 1000$  GeV and for a given value of  $M_\psi$ , other values of  $(y_\psi, y_U)$  that

<sup>2</sup> For  $s_h = 0.01$ , the extra factor in Eq. (16), namely,  $[\dots]^2 \approx [1 - 0.3 (1000 \text{ GeV} / M_U)(y_U / 5)]^2$ , with  $\Delta_{\phi,h} \ll 1$  and can be dropped. Thus, for  $s_h = 0.01$ ,  $y_U = 5$ ,  $M_U = 1200$  GeV, including the  $\phi$  contribution *decreases* the elastic cross-section to about a half.

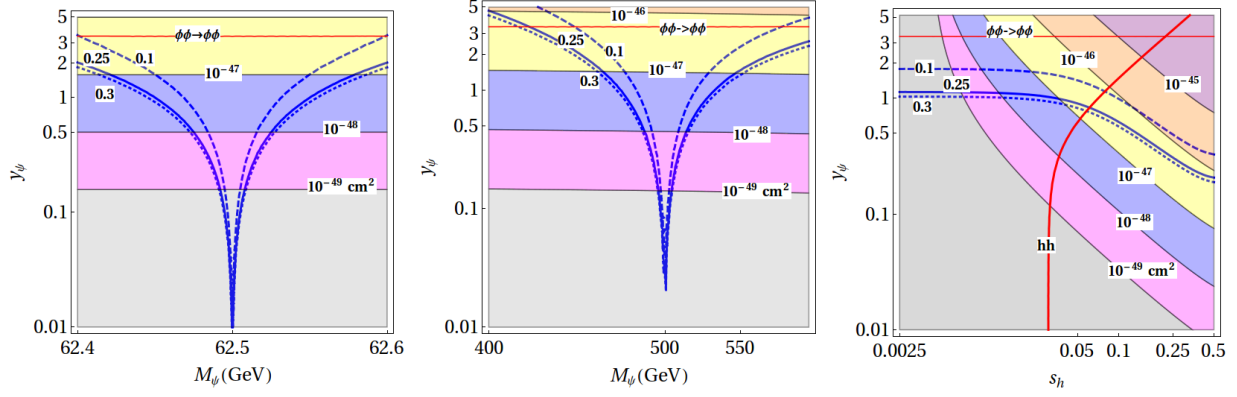


Figure 7: For  $Y_U = 2/3$ ,  $M_\phi = 1000$  GeV contours of  $\Omega_{dm} = 0.1, 0.25, 0.3$ , with the colored bands showing  $\sigma_{DD}$  as marked, for  $y_U = 5$ ,  $M_U = 1200$  GeV, and with the parameters not varied along the axes fixed at  $s_h = 0.01$  and  $M_\psi = 475$  GeV. The red horizontal line shows the unitarity constraint for  $y_U = 5$ , and the thick red line shows the 8 TeV LHC  $hh$  channel constraint.

give the correct relic-density and direct-detection rates can be obtained from those in Fig. 7, by scaling  $y_\psi \rightarrow (5/y_U)y_\psi$ . In summary, for  $s_h \ll 1$ , since the couplings of the dark matter with SM states is via loop-level effective couplings, we find that a fairly large value  $y_\psi y_U \approx 5$  is required in order for the dark matter self-annihilation cross-section to be of sufficient size to give the correct relic-density. Taking smaller values of  $y_\psi y_U$  will require tuning  $M_\psi$  closer to  $M_\phi/2$  (or to  $M_h/2$ ). The regions we identify are safe from present direct-detection constraints, and will be probed in upcoming experiments.

## 4 Conclusions

In this work, we analyze the possibility of a SM gauge-singlet vector-like fermion to be dark matter. This dark matter candidate couples to a SM gauge-singlet scalar with couplings to the SM sector via loop induced effective couplings to two-gluons or two-photons, or via the Higgs portal. We first study these in a model-independent manner and find the LHC direct constraints, LHC diphoton rate, and perturbative unitarity constraints as a function of the effective couplings. Following this, we analyze a new physics model with a singlet vector-like fermion, a singlet scalar, and a vector-like quark. The neutral vector-like fermion is absolutely stable and is identified as the dark matter. The singlet dark matter cannot couple to SM fermions directly, but rather couples to the SM sector via loop-level scalar-gluon-gluon and scalar-photon-photon effective couplings induced by the vector-like quark, and also via the Higgs-portal (due to Higgs-singlet mixing). We show that the  $hh$  channel at the LHC constrains the Higgs-singlet mixing to be very small ( $\lesssim 0.05$ ), and therefore the above mentioned loop-induced couplings are the most significant ones.

The effective couplings lead to the scalar mediated dark matter self-annihilation to the gluon-gluon and photon-photon final states (in addition to the higgs-higgs final state), scalar mediated dark matter direct-detection signal, and LHC scalar production via gluon-gluon fusion and its decay into the diphoton channel. These loop effective coupling processes are very important when the Higgs-singlet mixing is very small.

We compute the upper bound on the  $\phi$  coupling to the vector-like fermions requiring perturbative unitarity in the  $\phi\phi \rightarrow \phi\phi$  scattering channel. We show in Fig. 4 the range of diphoton signal cross-

sections obtained at the LHC by saturating the unitarity constraints for various singlet scalar widths and VLQ masses, which helps to give one an idea of the signal cross-sections possible at the LHC. The diphoton rate when the scalar-fermion couplings are varied is shown in Fig. 5. In addition to the direct production signals of the vector-like quark at the LHC, another promising mode is the  $\phi \rightarrow hh$  mode which already imposes very tight constraints on the parameter-space, although the size of this coupling is model dependent; models in which  $BR(\phi \rightarrow hh) \gtrsim 0.05$  may already be ruled out by the diHiggs LHC constraints.

We find that a fairly large value  $y_\psi y_U \approx 5$  is required in order to get a large enough self-annihilation cross section required to obtain the correct dark matter relic density. Furthermore,  $(M_\psi, M_\phi)$  needs to be in the pole enhanced region, i.e. within a few tens of GeV of  $M_\phi/2$  (or a few tenths of GeV of  $M_h/2$ ). We find regions of parameter space that are compatible with dark matter direct-detection bounds, and the direct-detection rate we find is accessible in current and upcoming experiments. We show these in Fig. 7, with the region consistent with the direct LHC  $hh$  bound and unitarity constraints also shown.

## A The $\kappa_{\phi\gamma\gamma}$ and $\kappa_{\phi gg}$ effective couplings

Here we provide the  $\kappa_{\phi gg}$  and  $\kappa_{\phi\gamma\gamma}$  effective couplings from Ref. [22] for easy reference. For the effective Lagrangian defined in Eq. (1), the 1-loop expressions for the  $\phi gg$  and  $\phi\gamma\gamma$  amplitudes  $\kappa_{\phi gg}$  and  $\kappa_{\phi\gamma\gamma}$  respectively, with  $\phi = \{h, H, A\}$  are given here. Defining  $r_f = m_f^2/m_\phi^2$  and with  $f$  running over all colored fermion species with mass  $m_f$  and Yukawa couplings  $y_{\phi ff}$ , and with the electric charge of the fermion ( $f$ ) denoted by  $Q_f$ , the general expressions for  $\kappa_{\phi gg}$  and  $\kappa_{\phi\gamma\gamma}$  are given as

$$\kappa_{\phi\gamma\gamma} = 2e^2 \sum_f N_c^f Q_f^2 \frac{y_{\phi ff}}{\sqrt{2}} \frac{M}{m_f} F_{1/2}^{(1)}(r_f), \quad \kappa_{\phi gg} = g_s^2 \sum_f \frac{y_{\phi ff}}{\sqrt{2}} \frac{M}{m_f} F_{1/2}^{(1)}(r_f), \quad (\text{A.17})$$

$$\text{with } F_{1/2}^{(1)}(r_f) = 4r_f \left( \int_0^1 dy \int_0^{1-y} dx \frac{g(x, y)}{(r_f - xy)} \right),$$

and  $g(x, y) = (1 - 4xy)$  for the CP-even scalars ( $h, H$ ) and 1 for the CP-odd scalar ( $A$ ). Here  $M$  is a mass scale which we set to 1 TeV for numerical results. The expressions for  $F_{1/2}^{(1)}$  in Eq. (A.17) match with the closed form expressions given in Ref. [23].

The color-factor in  $\kappa_{\phi gg}^{ab}$  is  $C_{ab} = (1/2)\delta_{ab}$ , where  $a, b = \{1, \dots, 8\}$  are the adjoint color indices. In the plots below and in App. A, we include this factor of  $(1/2)$  in the  $\kappa_{\phi gg}$  and suppress the color indices. Computing a decay rate or cross-section by summing over  $a, b$  gives  $\sum_{a,b} |C_{ab}|^2 = 8(1/2)^2 = 2$  resulting in a color-factor of 2.

## B Dark matter relic density

Here we give some details on the relic density calculation in the model we consider in this work. The  $|\mathcal{B}_i|^2$  for each of these final states are extracted from Ref. [7] to which we add  $|\mathcal{B}_{gg}|^2$  here. These

are given by

$$\begin{aligned}
|\mathcal{B}_{f\bar{f}}|^2 &= N_c^f y_f^2 y_\psi^2 s_h^2 c_h^2 \left(1 - \frac{4m_i^2}{s}\right) M_\psi^4 \hat{S}_{BW}^{h\phi} ; \quad \hat{S}_{BW}^{h\phi} = \frac{(M_\phi^2 - M_h^2)^2}{[(s - M_h^2)^2 + M_h^2 \Gamma_h^2] [(s - M_\phi^2)^2 + M_\phi^2 \Gamma_\phi^2]} , \\
|\mathcal{B}_{WW}|^2 &= \frac{1}{4} y_\psi^2 g^4 v^2 s_h^2 c_h^2 M_\psi^2 \left[ \frac{1}{2} + \frac{(s/2 - M_W^2)^2}{4M_W^4} \right] \hat{S}_{BW}^{h\phi} , \\
|\mathcal{B}_{hh}|^2 &= \frac{M_\psi^2 y_\psi^2}{64} \left\{ \frac{s_h^2 c_h^6 \kappa_{3h}^2 v^2}{[(s - M_h^2)^2 + M_h^2 \Gamma_h^2]} + \frac{c_h^8 \kappa_{\phi hh}^2 M_\phi^2}{[(s - M_\phi^2)^2 + M_\phi^2 \Gamma_\phi^2]} - \frac{2s_h c_h^7 \kappa_{3h} v \kappa_{\phi hh} M_\phi}{[(s - M_h^2)(s - M_\phi^2) + M_h M_\phi \Gamma_h \Gamma_\phi]} \right\} , \\
|\mathcal{B}_{gg}|^2 &= \frac{16y_\psi^2 M_\psi^6}{(16\pi^2 M)^2} \left\{ \frac{c_h^2 \kappa_{\phi gg}^2}{(s - M_\phi^2)^2 + M_\phi^2 \Gamma_\phi^2} + \frac{s_h^2 \kappa_{hgg}^2}{(s - M_h^2)^2 + M_h^2 \Gamma_h^2} - \frac{2c_h s_h \kappa_{\phi gg} \kappa_{hgg}}{[(s - M_h^2)(s - M_\phi^2) + M_h M_\phi \Gamma_h \Gamma_\phi]} \right\} ,
\end{aligned} \tag{B.18}$$

where  $s \approx 4M_\psi^2$ ,  $\hat{S}_{BW}^{h\phi}$  is a Breit-Wigner resonance factor including the s-channel  $\{h, \phi\}$  contributions,  $f\bar{f} = \{b\bar{b}, t\bar{t}\}$ , the  $\mathcal{M}_{ZZ}$  is identical to  $\mathcal{M}_{WW}$  except for an additional factor of  $1/(2c_W^2)$  and  $M_W \rightarrow M_Z$ , and in  $|\mathcal{M}_{hh}|$  we do not include the t-channel contributions as these are sub-dominant;  $M$  is a mass scale which we set to 1 TeV for numerical evaluations and the mixing angle  $\theta_h$  enters in  $\kappa_{\phi gg}$  and  $\kappa_{hgg}$  through  $\phi UU, \phi tt$  and  $htt$  couplings.

## References

- [1] I. Low, J. Lykken and G. Shaughnessy, Phys. Rev. D **84**, 035027 (2011) doi:10.1103/PhysRevD.84.035027 [arXiv:1105.4587 [hep-ph]].
- [2] M. J. Dolan, J. Hewett, M. Krmer and T. G. Rizzo, PoS DIS **2016**, 008 (2016).
- [3] D. Buttazzo, Frascati Phys. Ser. **61**, 108 (2016) [arXiv:1512.07576 [hep-ph]].
- [4] L. Lopez-Honorez, T. Schwetz and J. Zupan, Phys. Lett. B **716**, 179 (2012) doi:10.1016/j.physletb.2012.07.017 [arXiv:1203.2064 [hep-ph]].
- [5] S. Baek, P. Ko, W. I. Park and E. Senaha, JHEP **1305**, 036 (2013) doi:10.1007/JHEP05(2013)036 [arXiv:1212.2131 [hep-ph]].
- [6] M. A. Fedderke, J. Y. Chen, E. W. Kolb and L. T. Wang, JHEP **1408**, 122 (2014) doi:10.1007/JHEP08(2014)122 [arXiv:1404.2283 [hep-ph]].
- [7] S. Gopalakrishna, S. J. Lee and J. D. Wells, Phys. Lett. B **680**, 88 (2009) doi:10.1016/j.physletb.2009.08.010 [arXiv:0904.2007 [hep-ph]].
- [8] Y. G. Kim and K. Y. Lee, Phys. Rev. D **75**, 115012 (2007) doi:10.1103/PhysRevD.75.115012 [hep-ph/0611069].
- [9] Y. G. Kim, K. Y. Lee and S. Shin, JHEP **0805**, 100 (2008) doi:10.1088/1126-6708/2008/05/100 [arXiv:0803.2932 [hep-ph]].
- [10] The ATLAS collaboration, ATLAS-CONF-2015-081.
- [11] CMS Collaboration [CMS Collaboration], CMS-PAS-EXO-15-004;

- [12] S. Gopalakrishna and T. S. Mukherjee, arXiv:1604.05774 [hep-ph].
- [13] S. Bhattacharya, S. Patra, N. Sahoo and N. Sahu, arXiv:1601.01569 [hep-ph].
- [14] F. D’Eramo, J. de Vries and P. Panci, arXiv:1601.01571 [hep-ph].
- [15] Y. Mambrini, G. Arcadi and A. Djouadi, Phys. Lett. B **755**, 426 (2016) doi:10.1016/j.physletb.2016.02.049 [arXiv:1512.04913 [hep-ph]].
- [16] S. F. Ge, H. J. He, J. Ren and Z. Z. Xianyu, arXiv:1602.01801 [hep-ph].
- [17] H. Han, S. Wang and S. Zheng, arXiv:1512.07992 [hep-ph].
- [18] M. Backovic, A. Mariotti and D. Redigolo, JHEP **1603**, 157 (2016) doi:10.1007/JHEP03(2016)157 [arXiv:1512.04917 [hep-ph]].
- [19] G. Aad *et al.* [ATLAS Collaboration], Phys. Rev. D **92**, 092004 (2015) doi:10.1103/PhysRevD.92.092004 [arXiv:1509.04670 [hep-ex]].
- [20] J. Baglio and A. Djouadi, JHEP **1103**, 055 (2011) [arXiv:1012.0530 [hep-ph]].
- [21] D. de Florian *et al.* [LHC Higgs Cross Section Working Group], arXiv:1610.07922 [hep-ph].
- [22] S. Gopalakrishna, T. S. Mukherjee and S. Sadhukhan, Phys. Rev. D **93**, no. 5, 055004 (2016) doi:10.1103/PhysRevD.93.055004 [arXiv:1504.01074 [hep-ph]].
- [23] J. F. Gunion, H. E. Haber, G. L. Kane and S. Dawson, Front. Phys. **80**, 1 (2000).
- [24] A. M. Sirunyan *et al.* [CMS Collaboration], [arXiv:1611.03568 [hep-ex]].
- [25] S. A. R. Ellis, R. M. Godbole, S. Gopalakrishna and J. D. Wells, JHEP **1409**, 130 (2014) doi:10.1007/JHEP09(2014)130 [arXiv:1404.4398 [hep-ph]].
- [26] [ATLAS Collaboration], ATLAS-CONF-2013-018.
- [27] CMS Collaboration [CMS Collaboration], CMS-PAS-B2G-12-015.
- [28] V. Khachatryan *et al.* [CMS Collaboration], Phys. Rev. D **93**, no. 1, 012003 (2016) doi:10.1103/PhysRevD.93.012003 [arXiv:1509.04177 [hep-ex]].
- [29] The ATLAS collaboration, ATLAS-CONF-2016-013.
- [30] G. Aad *et al.* [ATLAS Collaboration], JHEP **1508**, 105 (2015) doi:10.1007/JHEP08(2015)105 [arXiv:1505.04306 [hep-ex]].
- [31] G. Aad *et al.* [ATLAS Collaboration], Phys. Rev. D **91**, no. 11, 112011 (2015) doi:10.1103/PhysRevD.91.112011 [arXiv:1503.05425 [hep-ex]].
- [32] V. Khachatryan *et al.* [CMS Collaboration], arXiv:1507.07129 [hep-ex].
- [33] V. Khachatryan *et al.* [CMS Collaboration], Eur. Phys. J. C **75**, no. 4, 151 (2015) doi:10.1140/epjc/s10052-015-3367-z [arXiv:1501.05603 [hep-ex]].
- [34] G. Aad *et al.* [ATLAS Collaboration], Phys. Rev. D **88**, no. 11, 112003 (2013) doi:10.1103/PhysRevD.88.112003 [arXiv:1310.6584 [hep-ex]].

- [35] K. Das and S. K. Rai, Phys. Rev. D **93**, no. 9, 095007 (2016) doi:10.1103/PhysRevD.93.095007 [arXiv:1512.07789 [hep-ph]].
- [36] A. Falkowski, D. M. Straub and A. Vicente, JHEP **1405**, 092 (2014) doi:10.1007/JHEP05(2014)092 [arXiv:1312.5329 [hep-ph]].
- [37] K. A. Olive *et al.* [Particle Data Group Collaboration], Chin. Phys. C **38**, 090001 (2014), doi:10.1088/1674-1137/38/9/090001.
- [38] M. E. Peskin and D. V. Schroeder, Reading, USA: Addison-Wesley (1995) 842 p
- [39] S. Gopalakrishna, A. de Gouvea and W. Porod, JCAP **0605**, 005 (2006) doi:10.1088/1475-7516/2006/05/005 [hep-ph/0602027].
- [40] A. Bharucha, A. Djouadi and A. Goudelis, arXiv:1603.04464 [hep-ph].
- [41] R. Adam *et al.* [Planck Collaboration], arXiv:1502.01582 [astro-ph.CO].
- [42] M. A. Shifman, A. I. Vainshtein and V. I. Zakharov, Phys. Lett. B **78**, 443 (1978). doi:10.1016/0370-2693(78)90481-1
- [43] G. Bertone, D. Hooper and J. Silk, Phys. Rept. **405**, 279 (2005) doi:10.1016/j.physrep.2004.08.031 [hep-ph/0404175].
- [44] H. Y. Cheng and C. W. Chiang, JHEP **1207**, 009 (2012) doi:10.1007/JHEP07(2012)009 [arXiv:1202.1292 [hep-ph]].
- [45] A. M. Green, Mod. Phys. Lett. A **27**, 1230004 (2012) doi:10.1142/S0217732312300042 [arXiv:1112.0524 [astro-ph.CO]]; C. McCabe, Phys. Rev. D **82**, 023530 (2010) doi:10.1103/PhysRevD.82.023530 [arXiv:1005.0579 [hep-ph]]; M. T. Frandsen, F. Kahlhoefer, C. McCabe, S. Sarkar and K. Schmidt-Hoberg, JCAP **1201**, 024 (2012) doi:10.1088/1475-7516/2012/01/024 [arXiv:1111.0292 [hep-ph]].
- [46] D. S. Akerib *et al.* [LUX Collaboration], Phys. Rev. Lett. **116**, no. 16, 161301 (2016) doi:10.1103/PhysRevLett.116.161301 [arXiv:1512.04756 [astro-ph.CO]]; D. S. Akerib *et al.* [LUX Collaboration], Phys. Rev. Lett. **118**, no. 2, 021303 (2017) doi:10.1103/PhysRevLett.118.021303 [arXiv:1608.07648 [astro-ph.CO]]; Rick Gaitskell, Vuk Mandic and Jeff Filippini, <http://dmttools.berkeley.edu/limitplots/>.